Green and easy synthesis of P-doped carbon-based electrocatalysts for the hydrogen evolution reaction

Sergio García-Dalí, Javier Quílez-Bermejo, Jimena Castro-Gutiérrez, Niki Baccile, María Izquierdo, Alain Celzard, Vanessa Fierro

Green and easy synthesis of P-doped carbon-based hydrogen evolution reaction electrocatalysts

Sergio García-Dalí[1,2], Javier Quílez-Bermejo[1,3], Jimena Castro-Gutiérrez[1], Niki Baccile[4], María T. Izquierdo[5], Alain Celzard[1,6], Vanessa Fierro[1]

[1]Université de Lorraine, Centre National de la Recherche Scientifique (CNRS), Institut Jean Lamour (IJL), F-88000, Épinal, France.

[2]Departamento de Ciencia de los Materiales e Ingeniería Metalúrgica, Universidad de Oviedo, 33004, Oviedo, Spain.

[3]Departamento de Química Inorgánica and Instituto de Materiales, Universidad de Alicante, Ap. 99, 03080, Spain

[4]Sorbonne Université, Centre National de la Recherche Scientifique, Laboratoire de Chimie de la Matière Condensée de Paris, LCMCP, F-75005 Paris, France.

[5]Instituto de Carboquímica (ICB-CSIQ), Miguel Luesma Castán 4, E-50018, Zaragoza, Spain.

[6]Institut Universitaire de France (IUF)

*Sergio García-Dalí. E-mail: sergio.garcia-dali@univ-lorraine.fr

*Vanessa Fierro. E-mail: vanessa.fierro@univ-lorraine.fr

Abstract

In this study, efficient electrodes for the hydrogen evolution reaction (HER) based on low-cost and metal-free carbon catalysts are presented. Phytic acid, a biosourced molecule containing carbon (C) and phosphorus (P), was found to be an excellent precursor for producing carbon materials with high P content, depending on the carbonization temperature, from 27.9 wt.% at 700 °C to 7.3 wt.% at 1000 °C. A green and easy route to produce P-doped carbon materials by heat treatment of this biosourced precursor without the need for additional reagents is thus proposed. We show that the conversion of P-O-type groups into P-C-type species is of paramount importance for improving the catalytic activity in HER of P-doped carbon materials. P-C-type groups appear to be the key factor in the electrocatalytic activity, reaching an onset potential of - 0.27 V. This study sheds light on the origin of the catalytic activity of P-doped carbons, in which P is expected to modify the homogenous distribution of the electron density of undoped carbons and increase their catalytic performance.

Keywords: Hydrogen evolution reaction; phosphorus-doped carbon; carbon doping.

1. Introduction

One of the main limitations of the hydrogen economy is the current large-scale hydrogen production, which is still obtained primarily from fossil fuels and coals. Indeed, 90% of hydrogen is produced by catalytic reforming of methane [1]. Electrochemical water splitting is emerging as an attractive alternative to produce H_2 gas on an industrial scale, as it occurs through the hydrogen evolution reaction (HER) in the cathode electrode while the oxygen evolution reaction (OER) takes place in the anode electrode. These reactions, by themselves, cause no greenhouse gas emissions and do not generate toxic byproducts [2–4]. Nevertheless, the HER exhibits sluggish kinetics and a high overpotential, which limits the large-scale hydrogen production.

To catalyze HER, it is customary to use noble metals, making the cost of these electrodes inaccessible to the general public [5,6]. The most commonly used noble metal for this purpose is platinum (Pt). Pt nanoparticles deposited on carbon supports are the state-of-the-art commercial electrocatalysts used in HER [7,8]. However, it is well-known that the use of Pt-based electrocatalysts cannot be implemented worldwide due to the scarcity, high cost, and low durability of this metal [9,10]. This makes it imperative to develop new materials with similar performance but at lower cost and with less environmental impact. Fe, Ni, or Co exhibit high catalytic performance [11–15] but, unfortunately, they are not without problems such as leaching of metal nanoparticles under reaction conditions, which reduces the durability and generates environmental concerns [16,17]. To address the shortcomings of metal-containing electrocatalysts, a new alternative based on metal-free carbon catalysts is emerging as efficient electrodes for HER, especially due to their low cost [18,19].

However, one of the main limitations of carbon materials as electrocatalysts is their low catalytic activity when undoped, as they have a homogeneous distribution of electron density

along the carbon layers, which reduces the performance of the materials. In order to tailor the properties by disturbing the electron density and increasing the catalytic activity, carbon materials are usually doped with heteroatoms. The most commonly used heteroatoms are N [20,21], O [22,23], S [24,25], B [24,25], and halogens [26,27], N being the most studied and well-known for its effect on electrocatalytic activity [28]. Compared to the mentioned heteroatoms, phosphorus (P) has received less attention as dopant for electrocatalysis of HER, and it has not even been studied in depth without the combination of other heteroatoms or metals for this purpose. Nevertheless, an emerging interest in P as a heteroatom in carbon materials has been raised in recent years in materials science to produce high-performance carbons. Incorporation of P into the carbon structure can have substantial effects on the chemical and physical properties in carbon materials. The presence of P modifies the electronic structure of carbons, thereby impacting the chemical reactivity of the material and altering the electrocatalytic properties [29–31]. Furthermore, the inclusion of P atoms in carbon materials has also been demonstrated to enhance the chemical and electrochemical stability, rendering them more robust against degradation and deactivation [32,33]. Consequently, P has been considered "the next heteroatom to be explored" by the scientific community [34].

There are three main methods to produce P-doped carbons [34]. The first route involves the carbonization of a carbon-containing precursor mixed with a phosphorus-containing compound [35]. The second route is based on the post-functionalization of a prefabricated carbon with a phosphorus-containing compound [36], and the third route involves the co-deposition of carbon and P from the gas phase [37]. Despite the high catalytic performance in a wide variety of applications achieved by these methodologies, all of these synthesis routes involve the use of environmentally unfriendly precursors, primarily phosphoric acid. An

alternative for the synthesis of highly active P-doped carbons through the use of biosourced precursors is thus needed [38].

Phytic acid, a C- and P-containing biosourced compound commonly found in legumes, cereals, and grains, has proven to be an excellent precursor for producing carbon materials with a high P content without the need for additional reagents [39]. However, many questions remain unanswered regarding the effect of heat treatment temperature on the carbonization of phytic acid and the consequences on HER performance. To better understand the effect of P species on HER and optimize P-doped carbon as electrocatalysts, phytic acid was thus carbonized at different temperatures to modulate the chemical state of P in the resultant carbon materials. The P-doped carbons were extensively characterized to conclude that the oxidation state of the P heteroatoms appears to be of paramount importance for HER catalytic activity. Moreover, this work proposes a green and easy route to produce P-doped carbon materials from a biosourced precursor with an excellent catalytic performance.

2. Material and methods

2.1 P-doped carbon synthesis

Phytic acid solution (50 % w/w H_2O), Pluronic® F-127, Nafion® (5 % w/w in H_2O), H_2SO_4 (98 %) and phosphate buffer solution (PBS) were purchased from Sigma Aldrich. Isopropanol (99.9 %) and potassium hydroxide (KOH, 85 %) were supplied by VWR. Guar gum was purchase from EKIBIO group. All reactants were used as received.

First, 4 g of phytic acid solution was mixed with 2 g of Pluronic® F-127 at 500 rpm for 1 h in an agate bowl (50 mL) with 10 agate balls (1 cm diameter), in a planetary ball-milling machine (PM100, Retsch). The reason for the presence of Pluronic® F-127 was to improve the processability of the phytic acid solution, which was too liquid, in order to obtain a paste of suitable consistency for mechanosynthesis. Traditional stirring methods were also applied

to obtain a homogenous mixture of both reagents. However, an efficient mixture of the precursors is only achieved through mecanosynthesis. The material obtained after mechanosynthesis was labelled as PA. Then, the PA sample was heat-treated in a tubular furnace at different temperatures (500, 600, 700, 800, 900, and 1000 ºC) for 1 h, with a heating rate of 5 ºC min^{-1} under an N_2 flow of 150 mL min^{-1}. Prior to the heat treatment, the furnace was purged at room temperature for 1 h under the same N_2 flow. The resulting carbon samples after heat treatment are named PA-x, where x stands for the heat-treatment temperature.

2.2 Physicochemical characterization

P-doped carbons treated at 500, 600, 700, 800, 900, and 1000 ºC were characterized by elemental analysis (EA), gas adsorption, X-ray diffraction (XRD), Raman spectroscopy, transmission electron microscopy (TEM), X-ray photoelectron spectroscopy (XPS), solid-state nuclear magnetic resonance (NMR), temperature-programmed desorption (TPD) and thermogravimetric (TG) analysis.

Direct determination of carbon, hydrogen, nitrogen, sulfur and oxygen contents (wt.%) was carried out using a Vario EL cube analyzer (Elementar), in which ~2 mg of each sample was burnt at 1700 ºC in an oxygen-containing helium atmosphere. In this elemental analysis (EA) apparatus, the gases generated by the combustion of the sample are separated through a chromatographic column and analyzed by a thermal conductivity detector, except for sulfur gases, which are determined using an infrared detector. The P content (wt.%) was determined by difference to 100, considering P as the only element apart from C, H, O, N, S.

N_2 adsorption-desorption isotherms were obtained at -196 ºC on a fully automated ASAP2020 manometric adsorption unit (Micromeritics). All adsorption experiments were performed after outgassing the samples under high vacuum (2 - 4 × 10^{-6} Pa), at 90 ºC for at

least 24 h in the degassing port. Additional degassing was performed in the analysis port for at least 6 h before introduction of successive doses of N_2, which began with the samples under high vacuum. Warm and cold volumes were measured after N_2 adsorption-desorption to avoid helium entrapment in the narrowest pores. For the materials synthesized at higher temperatures (800 – 1000 °C), *i.e.*, those with a more developed microporosity, H_2 adsorption-desorption isotherms at -196 °C were also obtained following the procedure described above. The BET area (A_{BET}) of the materials was obtained following the criteria recommended by IUPAC [40] using MicroActive® software (Micromeritics). Pore size distributions (PSDs) were obtained using SAIEUS® software (Micromeritics) to apply the 2D non-local density functional theory for heterogeneous surfaces (2D-NLDFT-HS) to the N_2 isotherms for PA-500, PA-600, and PA-700 materials, and to the N_2 and H_2 isotherms for PA-800, PA-900, and PA-1000 materials. The total surface area (S_{NLDFT}) was then calculated from the PSD of each material.

The Bruker D8 Advance A25 polycrystalline powder X-ray diffractometer was used to determine the structural order of all carbons. The device is equipped with an X-ray source with a Cu anode (operating at 40 kV and 40 mA), a scintillation detector, and a graphite monochromator. Silver behenate was used as reference. In addition, Raman spectra were acquired with a Horiba Scientific XploRa Raman spectrometer using a long-range 50× objective and a red laser light (wavelength 638 nm, circularly polarized and filtered to 1 % of its nominal power) dispersed using a holographic grating (1200 lines mm^{-1}). Each spectrum presented in this work is an average of 7 spectra obtained on 7 different areas of each sample, and each of these 7 spectra is itself the result of the accumulation of 2 successive spectra acquired during 180 s on a range of Raman shifts between 800 and 2200 cm^{-1}. The final spectra were finally fitted according to the method described by Mallet-Ladeira et al. [41]

using a double Lorentzian for the D band and an asymmetric mixed Gaussian−Lorentzian profile for the G band.

TEM images were acquired in a JEM – ARM 200 F Cold FEG TEM/STEM equipped with probe and image spherical aberration correctors. To prepare the samples, the powdered material was dispersed in ethanol by low-power sonication. Then, a drop of the resulting suspension was deposited on a carbon-coated copper TEM grid (200 mesh) and air-dried.

XPS spectra were obtained using an ESCAPlus OMICRON spectrometer equipped with a non-monochromatized MgKα X-ray source. Shirley-type background subtraction, peak fitting, and quantification were processed using CASA software.

^{31}P and ^{13}C solid-state NMR experiments were performed on a Bruker Avance III HD operating under 7.05 T ($\nu(^{1}H)$ = 300 MHz) spectrometer and equipped with a 4-mm magic angle spinning (MAS) probe. The ^{31}P and ^{13}C NMR spectra were obtained by direct magnetization transfer under MAS without proton decoupling with ν_{MAS} = 12.5 kHz. For ^{31}P, the experimental conditions were as follows: number of transients between 128 (T = 500 °C) and 21430 (T = 1000 °C), time-domain size TD = 1 k, pulse length $p(^{31}P)$ = 1.00 µs, relaxation delay D = 5 s. For ^{13}C, the experimental conditions were as follows: number of transients 250, time-domain size TD = 352, pulse length $p(^{13}C)$ = 3.62 µs, relaxation delay D = 20 s.

To follow the mass loss and decomposition processes during carbonization, the PA sample was studied by thermogravimetric (TG) analysis. The sample was heated to 1000 °C with a heating rate of 10 ºC min^{-1} in a continuous flow (50 mL min^{-1}) of Ar. Temperature-programmed desorption (TPD) measurements were performed following the m/z lines of 18 (H_2O), 28 (CO) and 44 (CO_2) to further understand the surface chemistry of the materials. The thermobalance was purged via three vacuum – Ar cycles to ensure an inert atmosphere during

the experiments. Then, the materials are heat-treated at 900ºC with a heating rate of 10ºC min^{-1}. Ar flow was kept constant at 50 mL min^{-1} during TPD measurements.

2.3 Electrochemical measurements

The P-doped carbons were electrochemically characterized in a traditional three-electrode cell with a rotating ring-disk electrode (RRDE) connected to a PGSTAT302N bi-potentiostat (Metrohm). The working electrode consists of a glassy carbon disk (0.196 cm^2) and a platinum ring as a second working electrode. A reversible hydrogen electrode (RHE) was used as the reference electrode and a glassy carbon rod (8 mm diameter) as the counter electrode. Electrochemical measurements were performed in an acidic electrolyte (0.5 M H_2SO_4) at room temperature. The catalytic activity for the HER was also assessed for the most catalytic material in N_2-saturated 1 M KOH and PBS solutions, for comparison purposes. To prepare the working electrodes, the P-doped carbons were suspended (4 mg mL^{-1}) in an isopropanol/water (20/80, v/v) solution with 0.2 wt.% of Nafion®. Then, 4 aliquots of 8.42 µL of the resulting ink were drop-cast onto the glassy carbon disk, reaching a carbon loading of 0.68 mg·cm^{-2}. To achieve maximum wettability of the prepared electrodes, all materials were immersed in the working solution under vacuum for a few minutes, according to the optimized method for electrode preparation [42]. Then, each electrode was introduced into the working solution under continuous nitrogen bubbling. Prior to the electrocatalytic study, to stabilize the electrode, cyclic voltammetry (CV) scans from 1.00 to 0.00 V vs. RHE were recorded at a scan rate of 50 mV s^{-1} (20 cycles). Then, linear sweep voltammetry (LSV) measurements were carried out at 1600 rpm with a scan rate of 5 mV s^{-1} from 0.20 V to -0.80 V vs RHE. The currents were always normalized by the geometric area of the disk (0.196 cm^{-2}). The potential required to reach -10 mA·cm^{-2} (hereafter referred to as E_{HER}), as well as the overpotential, which is the extra potential required to activate the electrochemical reaction at

an electrode interface, was used to compare the catalytic activity of the PA materials. In the case of HER, the theoretical potential is 0.00 V vs. RHE (Equation 1).

$$2H^+ + 2e^- \rightarrow H_2 \qquad \text{Eq.1}$$

Electrochemical impedance spectra were also recorded for all samples in the frequency region between 100 kHz and 100 mHz with a voltage amplitude of 10 mV at a fixed potential of 0.5 V vs. RHE. The stability of the material under working conditions was evaluated through 1000 LSV repetitions. Furthermore, the stability under aggressive conditions was also evaluated through chronoamperometric tests, which were performed at the potential in which a current density of - 5 mA cm^{-2} is reached in LSV curves. Then, this fixed potential was maintained for 5000 s. A commercial platinum-based electrocatalyst (Pt/C, from Sigma-Aldrich) was also evaluated under the same conditions in the electrocatalytic experiments for comparison purposes.

3. Results and discussion

Figure 1 illustrates the easy and green synthesis process to obtain the PA-x series of P-doped carbons after carbonizing the sample PA at different temperatures. The carbonization yields are shown in Table 1. As expected, the higher the heat treatment temperature, the lower the carbonization yield, from 37 % at 500 ºC to 7 % at 1000 ºC. At temperatures above 1000 ºC, no carbon was obtained after the heat treatment. Carbonization yields obtained from the highest temperature exhibit lower values compared to the carbonization of other carbon

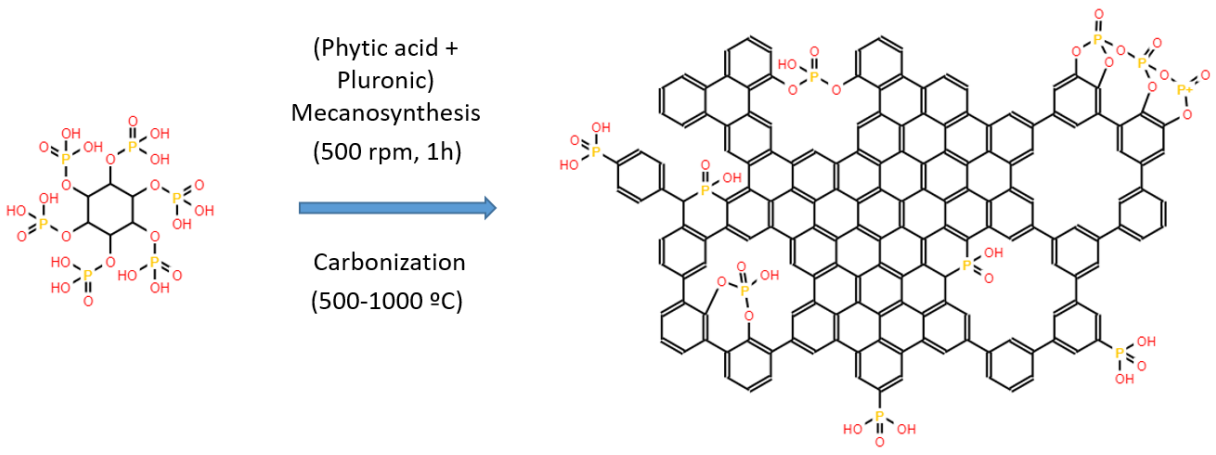

precursors. However, phytic acid serves as a low-cost phosphorus and carbon-containing precursors that avoids the use of other costly reagents, thereby rendering PA-derived carbons as a promising class of low-cost P-doped carbon materials. Table 1 also gathers the carbon, oxygen, phosphorus, and hydrogen contents determined by elemental analysis. As observed, the heat treatment temperature plays a key role in the heteroatom content of the carbon materials, as the oxygen and phosphorus contents clearly vary with temperature.

Figure 1: Schematic of the synthesis process of P-doped carbons from phytic acid.

Table 1: Carbonization yield (%), mass contents (wt.%) of carbon (C), oxygen (O), hydrogen (H), and phosphorus (P) obtained by elemental analysis, BET (A_{BET}) and 2D-NLDFT-HS (S_{NLDFT}) areas from adsorption isotherms, and I_D/I_G ratio calculated from Raman spectra for all PA-x materials.

Sample	**Carbonization yield**	**C**	**O**	**H**	**P**	**A_{BET} / S_{NLDFT}**	**I_D/I_G ratio**
	%	wt%	wt%	wt%	wt%	$m^2\ g^{-1}$	-
PA-500	37	21.3	56.3	3.5	19.0	0/0	0.78
PA-600	35	33.3	46.3	3.6	16.8	10/8	0.84
PA-700	33	35.7	34.6	2.0	27.9	13/11	0.84
PA-800	13	51.8	30.5	1.7	16.0	211/219	0.85
PA-900	10	64.3	23.3	1.2	11.2	723/820	0.94
PA-1000	7	77.0	15.1	0.6	7.3	960/1092	0.96

The oxygen content decreases with temperature, while the P content initially increases to a maximum at 700 ºC, due to the combination of removal of oxygen and hydrogen groups and carbon enrichment, and then decreases at higher temperatures.

The A_{BET} values were very different depending on the carbonization temperature. At temperatures below 800 ºC, the materials show N_2 isotherms (Figure 2a) typical of non-porous or very low surface area-materials, as corroborated by the values reported in Table 1. However, there is a significant and progressive increase in A_{BET} at temperatures at and above 800 °C, *i.e.*, 211 $m^2 g^{-1}$ at 800 ºC, 723 $m^2 g^{-1}$ at 900 ºC, and 960 $m^2 g^{-1}$ at 1000 ºC (Figure 2b). The gas evolution increases with temperature, leading to the development of porosity in the PA-derived carbon materials (see PSDs in Figure 2c), hence the observed increase in A_{BET}. S_{NLDFT} was slightly higher than A_{BET} due to the development of ultramicropores, less than 0.7 nm wide, for which the BET method underestimates the surface area [43]. It is important to note the widening of the knee in the N_2 isotherms at $p/p_0 > 0.05$ indicating the increase in supermicropores, between 0.7 and 2 nm wide with the carbonization temperature. Indeed, this is reflected in the widening of the PSDs (see again Figure 2c) that should facilitate the diffusion of ions and gases to and from the surface, respectively.

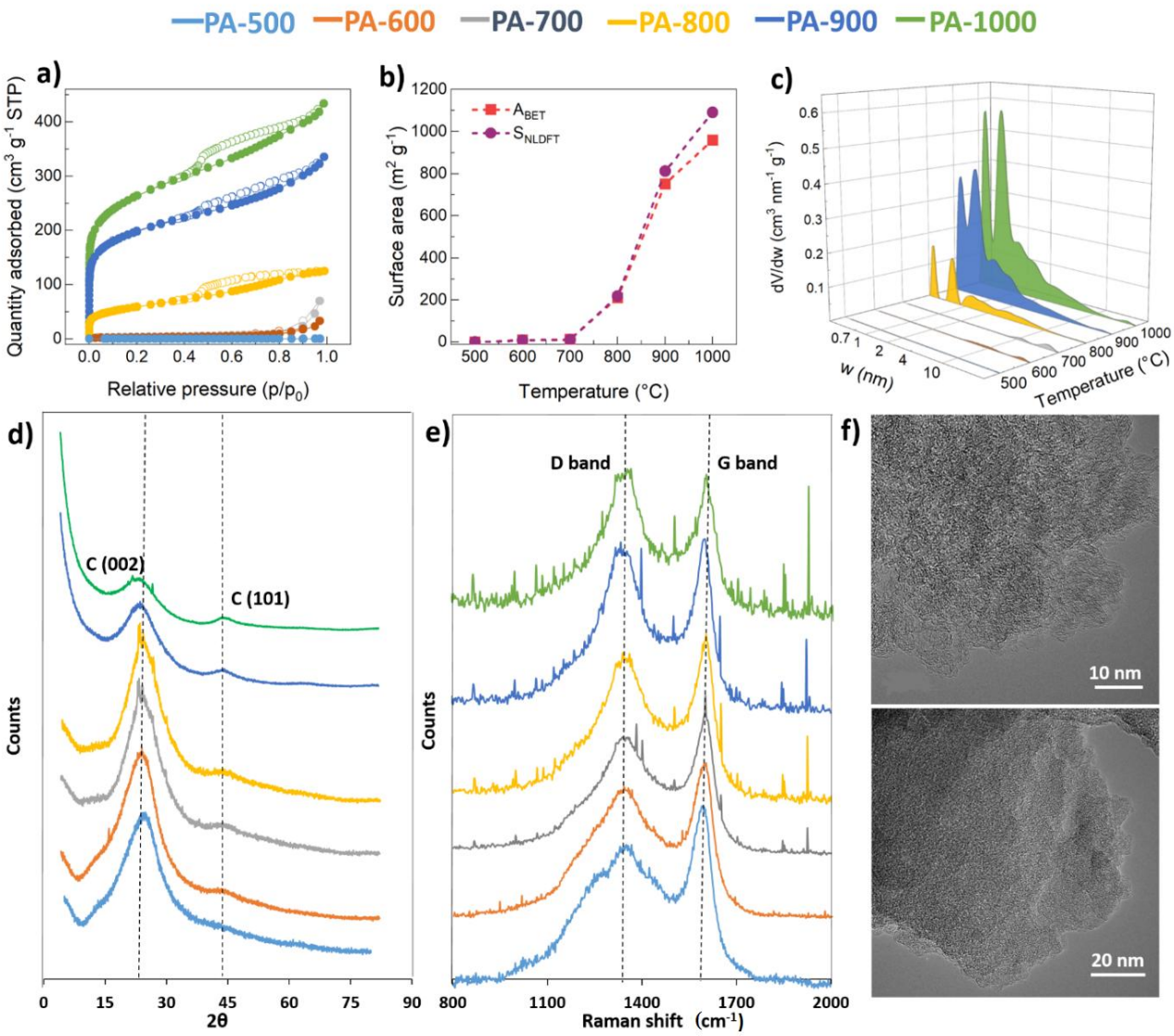

Figure 2: a) N_2 adsorption (full symbols) – desorption (empty symbols) isotherms; b) Surface area; c) Pore size distribution; d) XRD patterns; and e) Raman spectra of PA-based materials treated at different temperatures. f) TEM images of PA-900.

The XRD patterns of the P-doped carbon materials synthesized at different temperatures are shown in Figure 2d. All samples exhibit an XRD pattern with a broad (002) diffraction band centered at 2θ = 23º, which is attributed to highly disordered carbons in which the more or less parallel aromatic carbon sheets are randomly twisted with respect to each other. With the increase of the heat treatment temperature from 600 to 1000 ºC, a second diffraction band appears centered at 2θ = 43º. This second band, (101), is related to the appearance of order in

the planar direction, suggesting that the high-temperature heat treatment leads to the formation of graphitic domains in the carbon structure [44].

The Raman spectra of the P-doped carbons in Figure 2e exhibit two main bands characteristic of carbon materials. The D band, which appears at around 1350 cm^{-1}, is attributed to defects within the carbon layers and to heteroatoms, and the G band, which appears at 1590 cm^{-1}, corresponds to the C-C elongation mode in the aromatic rings, and therefore to the vibrations of sp^2 carbons. However, the ratio of the intensities of the D and G bands, I_D/I_G, can only be used as an indicator of graphitization if the carbon materials under study are actually graphitizable. In the present case, with precursors rich in oxygen and containing only sp^3 carbons, the heat treatment leads to an increase in the I_D/I_G ratio and a shift of the G band towards 1600 cm^{-1}, i.e., the opposite behavior of what is observed with 100% sp^2 carbons for which only the dimension of the coherent domains, L_a, varies. This regime called "carbonization" as opposed to the regime called "graphitization" [45], is indeed such that the I_D/I_G ratio is no longer proportional to $1/L_a$, but to L_a^2 [46]. For these materials, an increase of the I_D/I_G ratio thus corresponds to an increase in the size of L_a, although the latter remains very small. The observed increase in the I_D/I_G ratio (Table 1), from 0.78 at 500 ºC to 0.96 at 1000 ºC after deconvolution of the general profile, is therefore indicative of a higher ordering at the nanoscale, in agreement with the XRD results. This finding is also corroborated by the shift to higher values of the G band in the samples obtained at higher temperatures, in line with the 2nd stage of the ordering trajectory described by Ferrari an Robertson [47]. TEM images of P-doped carbons are shown in Figure 2f (PA-900) and Figure S1. In all cases, a typical highly disordered carbon with a worm-like nanoporosity was observed.

The XPS spectra of all PA-derived carbon materials were performed to study the surface chemical changes occurring during heat treatment. The carbon, oxygen and phosphorus contents in the surface chemistry of the materials is gathered in Table S1. Interestingly, the P content on the carbon surface decreases with the temperature of the heat-treatment and the maximum at 700 ºC observed by elemental analysis is not present. The differences between the chemical composition in the bulk (see Table 1) and the surface chemistry (Table S2) suggest that there is a higher concentration of P in the bulk of PA-700, which produces an increase in the porosity of the material when part of this P is removed at 800 ºC, as observed in the adsorption isotherms (Figure 2a). Figure 3 shows the P 2p XPS spectra of the whole PA-x series. At the lowest temperatures, 500 – 600 ºC, the carbon materials exhibit a single peak at 134.2 eV, which is related to C-O-P species, specifically C-O-PO_3-type groups [48]. After heat treatment at temperatures above 700 ºC, a new peak appears at 133.0 eV, which is

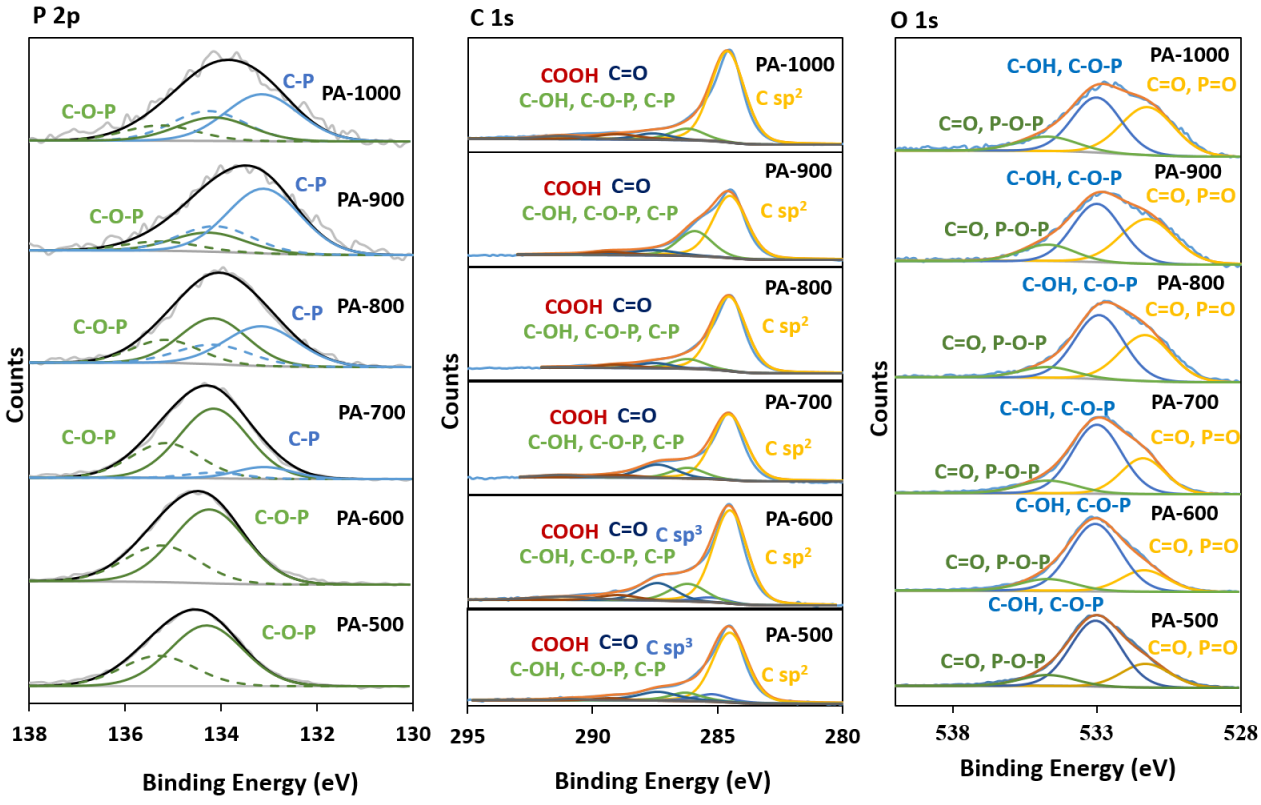

attributed to C-P species bound to one or two carbon atoms (*i.e.*, C-PO_3 or C_2-PO_2, respectively).

Figure 3: XPS spectra of P 2p (left column), C 1s (middle column) and O 1s (right column) of each PA-x material.

Interestingly, Figure 3 shows that the higher the heat treatment temperature, the larger the contribution of the C-P peak, reaching a maximum at 900 ºC. These results indicate that there is a conversion of the C-O-P groups into C-P species at high temperatures. Nevertheless, for PA-1000, the C-P species do not seem to be stable, since there is a significant decrease in the C-P peak compared to that of PA-900.

The C1s spectra are also shown in Figure 3, where an intense peak at 284.7 eV, related to graphitic carbon (sp^2 hybridization), and a second smaller peak at 285.2 eV, associated with aliphatic carbon (sp^3 hybridization) [49], are observed. The latter only appears when the temperature of the heat treatment is not high enough to complete the formation of graphitic domains (500 and 600 ºC), as suggested by Raman and XRD experiments. At temperatures above 600 °C, the C1s spectra show a greater contribution from sp^2 hybridization, and peaks related to alcohol or C-O-P groups (286.2 eV), carbonyl groups (287.5 eV), and carboxylic or esters groups (289.0 eV) are also identified [50]. In the P-doped carbon materials obtained at the lowest temperatures, there is a high contribution of C-O-type species, which decreases at temperatures above 800 ºC, while the contribution of C-P species is also observed at such a temperature, in agreement with the P 2p spectra [51]. The O 1s XPS spectra show characteristic peaks of C=O or P=O bounds (531.2 eV), as well as C-O-H or C-O-P groups (533.2 eV) and C-O aromatic or P-O-P groups at 534.5 eV [52].

The ^{31}P and ^{13}C solid-state MAS-NMR spectra of the PA-x materials and the PA sample are shown in Figure 4a. The ^{13}C spectra of all heat-treated samples are characterized by a broad signal at 127-130 ppm, typical of conjugated sp^2 bonds as found in condensed aromatic systems [53], which clearly contrasts with the spectrum of PA, characterized by signals

attributed to OCH_x species around 70 ppm (expected in both PA and Pluronic® F-127) and CH_3 of Pluronic® F-127 at 16 ppm. The ^{13}C spectra nicely corroborate the formation of -C=C- bonds in the carbon samples, previously suggested by XRD and Raman spectroscopy.

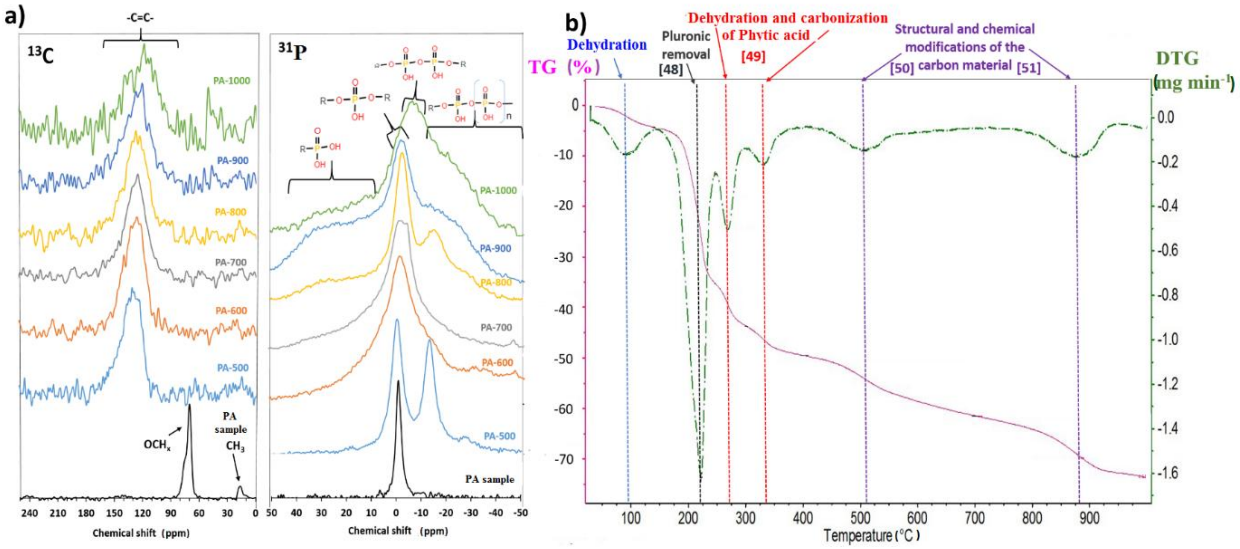

Figure 4: a) ^{13}C (left) and ^{31}P solid-state MAS-NMR (right) spectra of PA-x materials: b) TG plots and their derivatives (DTG) of the PA sample.

On the other hand, all ^{31}P spectra show broad resonance peaks in a broad range of chemical shifts, indicating the wide variety of P-containing species and the chemical environment of the P-doped carbons. The main resonance peak, which appears around 0 ppm, is in the spectral region of phosphate mono- (from 0 to +10 ppm) and di-esters (from 0 to -5 ppm) [54,55]. PA exhibits the characteristic signal of phytic acid [56], while all PA-x materials show the presence of phosphate esters. The presence of C-P species (phosphonate groups) in the carbon materials obtained at temperatures above 800 ºC is corroborated by the broad ^{31}P signal above 10 ppm [54,55], while pyro- (from -5 to -15 ppm) and poly-phosphates (from -15 to -30 ppm) [54,55] are produced at all temperatures, as evidenced by the more or less defined peak at around -14 ppm (e.g., for PA-500 and PA-800) and spurious peaks observed between -45 and -50 ppm (e.g., for PA-600 and PA-700).

It is well-known that polyphosphate groups are obtained from the conversion of phosphoric groups at high temperatures [57], and the wide range of polyphosphate-like species in PA-900

and PA-1000 and their high stability at these temperatures suggest that these polyphosphate chains may not be connected to one but to several carbon atoms in the carbonaceous matrix. The pyrophosphate groups produced at lower temperatures (PA-500) have their peak vanishing at 600 ºC, suggesting that these unstable pyrophosphate groups are connected exclusively to the chain end, contrary to the pyrophosphate groups generated at 800 ºC.

The TG/DTG plots of the PA sample are shown in Figure 4b. The first mass loss, due to water removal, occurs at T_{peak} = 86 ºC and is equal to 4.2 %. Then, a large mass loss (29.9 %), presumably due to Pluronic® removal [58], is observed at T_{peak} = 222 ºC. Interestingly, such mass loss should be 50 wt.%, taking into account that the weight ratio of PA and Pluronic® in the initial weight paste was 1:1. The lower mass loss of the Pluronic® (29.9 wt.%) could be related to the presence of hydroxyls groups in Pluronic®, which might favor condensation reactions with phosphate groups in PA, similar to that reported in the activation of cellulose with phosphoric acid [59]. Two subsequent peaks, corresponding to the dehydration and carbonization process of phytic acid [60], appear at 268 ºC and 330 ºC, with a mass loss of 8.2 and 5.6 %, respectively. Interestingly, at 506 and 876 ºC, two significant mass losses are observed, which can be directly related to the structural and chemical changes of the PA-derived carbon materials. From the ^{31}P-NMR spectra, the first mass change (506 ºC) can be related to the removal of pyrophosphate-type groups [61] observed in PA-500, as these peaks are no longer observed in PA-600. The second mass loss (876 ºC) could be attributed to two different processes: (i) the removal of CO_2 from oxygenated groups present in the carbon [62], which creates micropores and produces the drastic observed increase in A_{BET}; and (ii) the elimination of pyrophosphate groups, as well as the generation of polyphosphate chains and phosphonate groups, evidenced by the ^{31}P-NMR spectra.

The oxygen content of PA-900 and PA-1000 is substantially high compared to other carbon materials obtained at similar temperatures. To deepen into the oxygen chemistry, TPD

experiments were performed for PA-900 and the results are shown in Figure S2. The desorption of surface oxygen groups by TPD is a well-known process, in which CO evolution is related to the decomposition of neutral and basic oxygen groups, such as phenols and carbonyls, while CO_2 evolution is useful for the characterization of acid groups, such as carboxylic or lactone groups. In the case of PA-900, TPD-profile shows a large contribution of CO desorption at temperatures above 700ºC, which is often related to a high content in carbonyl and phenol groups [62]. However, the CO evolution at temperatures close to 900ºC has also been attributed to the presence of C-O-P-type bonds [63,64], which aligns with the decrease of C-O-P-type bonds observed by XPS at these temperatures (Figure 3). It should be noted that no peak in CO emission is observed, suggesting that stable groups responsible for CO evolution may continue to desorb at even higher temperatures. CO_2 and H_2O TPD-profiles show that the oxygen groups of PA-900 does not appear to be associated with the presence of acid groups or adsorbed water. The oxygen content determined by TPD was 16 wt.%, in agreement with XPS results.

Based on the results obtained from the physicochemical characterization of the PA-x series of materials, a carbonization mechanism of phytic acid is proposed. Figure 5 shows a schematic representation of the proposed evolution of the carbon structure and the P species present in the P-doped carbons obtained at different temperatures. It should be noted that the schematic does not represent the tridimensional conformation of the materials and therefore porosity is not shown. At 500 ºC (PA-500), dehydration and carbonization processes have taken place, and a disordered macroporous carbon material with a predominance of phosphate di-ester and pyrophosphate groups is obtained. Between 700 and 800 ºC, significant structural changes are observed in the PA-derived carbon materials, as the textural properties are significantly modified by the formation of micropores, and graphenic domains start to form. Furthermore, the conversion of P-O-type groups into P-C species begins to be observed. At

900 ºC (PA-900), the maximum contribution of P-C species is observed, while a wide variety of polyphosphate chains are identified, probably through interaction with carbon atoms along the structure. At the highest temperature (PA-1000), some of the P-C species are removed from the surface of the materials, while the highest surface area and number of nano-graphenic domains are found.

Significant differences are observed between the results of XPS and NMR techniques, but this is due to the fact that XPS is a surface-dependent characterization technique, while NMR covers both bulk and surface chemistry. Combining the results of the two techniques thus shows that P-doped carbons are essentially composed of a core of condensed aromatic structures and a surface rich in O functional groups, such as COH and COOH, and P functional groups, such as pyrophosphates, polyphosphates and phosphonates.

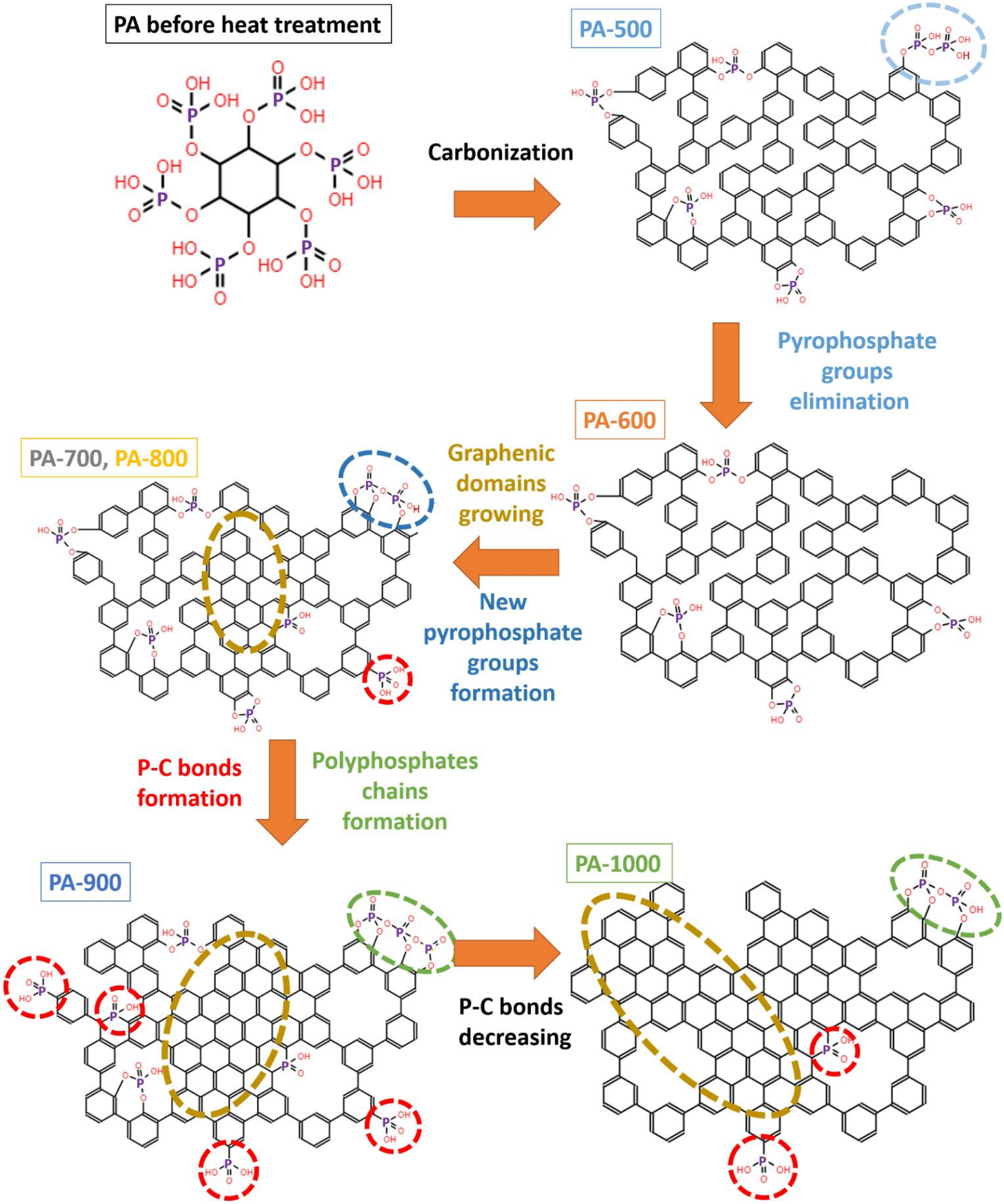

Figure 5: Schematic of the proposed evolution of the P-doped carbon as a function of temperature. Dashed circles emphasize the chemical modifications (same colors as the text in the Figure) at each temperature.

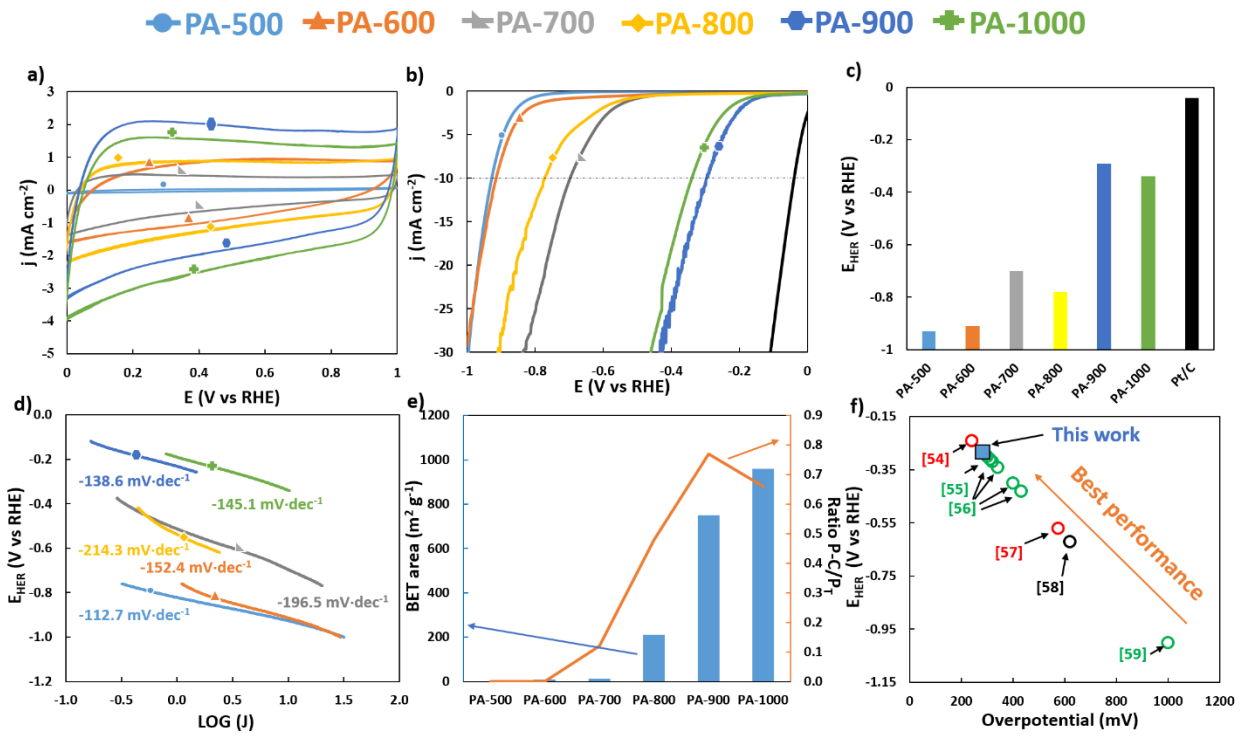

Figure 6: a) Cyclic voltammetries, and b) linear sweep voltammetries in a 0.5 M H_2SO_4, N_2-saturated solution at 50 mV s^{-1} of the as-prepared P-doped carbons and the commercial Pt/C (black line); c) Graphical representation of the E_{HER} values of the P-doped carbons and the commercial Pt/C; d) Tafel slopes of all P-doped carbons in 0.5 M H_2SO_4; e) Graphical representation of BET area (blue bars) and (P-$C_{species}$) /P_T atomic ratio (orange line); f) Literature comparison of the HER performance of similar materials (unfilled circles: red for N-doped carbons, green for P-doped carbons, and black for undoped-carbon) to PA-900 (blue solid square).

Figure 6a shows the CV profiles of all PA-x materials in a 0.5 M H_2SO_4 aqueous, N_2-saturated solution at 50 mV s^{-1}. The CV profile of PA-500 and PA-600 shows a negligible contribution from the double layer, which is explained by their negligible surface area (see again Table 1). After heat treatment at temperatures above 700 ºC, carbonization produces gas evolution leading to the creation of micropores and, as a consequence, to higher surface area and capacitance values. In addition, the typical rectangular CV profile of these materials, obtained at temperatures above 700 ºC, is characteristic of carbon materials with well-developed porous textures. Moreover, an increase in the electrical conductivity of the materials could also explain such an increase in the double-layer capacitance. Furthermore, the electrochemical impedance spectroscopy (EIS) was performed in all samples, as shown in Figure S3. The EIS-profiles display a more pronounced slope at low frequencies in the Nyquist plot with the temperature treatment. The diffusion of the species in an

electrochemical system becomes slower as diffusion resistance increases, which is related to the slope at low frequencies in the Nyquist plot [65]. Therefore, the steepest slope in the Nyquist plot of PA-900 is attributed to the lowest diffusion resistivity compared to other PA-derived carbon materials. To further explore the electrical conductivity of the samples, an inset of the EIS plot focusing on the 25-25 Ω range is presented in Figure S3. The EIS exhibit typical characteristics observed in carbon materials. The behavior observed in the medium to high-frequency range for the samples synthesized at lower temperatures indicates poor electrical conductivity and limited charge propagation [66]. Conversely, the materials synthesized at temperatures above 800ºC display a steeper slope in the corresponding region of the Nyquist plot, indicating improved charge propagation.

The electrochemical performance for HER was evaluated for all P-doped materials. The electrocatalytic activity of the P-doped carbons was carried out in an N_2-saturated acidic electrolyte (0.5 M H_2SO_4) by linear sweep voltammetry (LSV) and the results are shown in Figure 6b. The HER performance of the commercial Pt/C (black curves in Figures 6a and 6b, and black bar in Figure 6c) was included for comparison. We observed that the higher the pyrolysis temperature, the higher the E_{HER} and thus the better the electrocatalytic performance towards HER. At the lowest temperatures, the catalytic behavior of the materials remains far from the state-of-the-art performance of commercial electrodes, with poor E_{HER} values around -0.87 V vs RHE in the case of PA-500 and PA-600. However, once the heat treatment temperature increases, an improvement in catalytic activity is observed, increasing the performance to the highest level at 900 ºC, with an E_{HER} of -0.27 V vs RHE for PA-900 (Figure 6c). Moreover, PA-900 has also been tested towards HER under both basic (1 M KOH) and neutral (PBS solution) conditions, as shown in Figure S4. The catalytic activity of PA-900 in KOH and PBS solutions exhibits a substantial decline, with an E_{HER} of -0.50 V vs RHE in KOH while E_{HER} is not achieved in the PBS solution in the entire potential range.

This observation could be attributed to the different oxidation states of C-P active sites in operando. In an acid electrolyte, the C-P, in the form of C-O-PO_3, is assumed to be protonated by H_3O^+ cations present in the solution. Previous research has demonstrated that the presence of H_3O^+-containing solution may alter the nature of the active sites in carbon electrocatalysts, leading to different reaction kinetics and mechanisms [67]. In KOH and PBS, the oxidation states of C-P species may differ based on the pH, resulting in lower HER kinetics. Furthermore, carbonization of PA was also performed in the absence of Pluronic® (PA-900 WP), as well as in the presence of a greener binder, the Guar gum (PA-900 GG). These materials were tested toward HER (Figure S5). LSV curves show a lower electrocatalytic activity in PA-900 GG (E_{HER} of -0.60 V vs RHE) and a negligible activity in PA-900 WP, suggesting that the presence of Pluronic® plays a key role in the carbonization of phytic acid by inducing significant changes in the PA-derived carbon materials. Further research is required to deepen into this matter and to better understand the role of Pluronic in the phytic acid carbonization.

Tafel slopes provide insight about the rate-determining step, which can give information about the different active sites in these materials. Figure 6d shows the Tafel slopes for the HER in 0.5 M H_2SO_4 solution. All materials show Tafel slopes from -112 to -214 $mV \cdot dec^{-1}$, which indicates that water adsorption (Volmer step) is the rate-determining stage in the HER mechanisms [68]. As observed, the P-doped carbons obtained at the highest temperatures are those that exhibit more positive Tafel slopes. Moreover, the Tafel slopes decrease to more negative values with the increase in temperature, from PA-500 to PA-800, probably due to the removal of phosphoric groups that confer hydrophilicity to the material. The similar Tafel plots of the materials obtained at low temperature and the undoped carbon materials suggest the same carbon-based active sites. It is worth mentioning here that PA-500 disrupts the trend previously mentioned by showing a Tafel slope of -113 mV dec^{-1}. Nevertheless, this material

has still not developed large textural properties, which make it non-attractive for future application. The most positive Tafel slopes of PA-900 and PA-1000 point out the different HER rate determining step in these materials and the higher kinetics compared to those obtained at lowest temperatures. Therefore, changes in the surface chemistry of these materials with heat treatment temperature led to different active sites and reaction mechanisms. However, a deeper modification in the chemistry or in the textural properties in the material are need if a further decrease in Tafel slope is desired.

In order to clarify the key factors influencing the electrocatalytic behavior of the as-prepared P-doped carbons, a graphical representation of A_{BET} and the ratio of P-C-type species (P-$C_{species}$) to total phosphorus (P_T) obtained from XPS, *i.e.*, the atomic ratio (P-$C_{species}$)/P_T, is shown in Figure 6e and Table S1. The highest HER catalytic performance was obtained with the carbons prepared at the highest temperatures, which is in agreement with the largest value of A_{BET}. However, PA-1000, which has the highest A_{BET}, has a lower electrocatalytic activity than PA-900. Interestingly, PA-900 presents the highest content of P-C-type species, indicating that this factor plays a key role in the electrochemical activity. The P atom has a lower electronegativity than the C atom, meaning that P in P-C-type species exhibits electron-donating properties, leading to a higher electron density of the C adjacent to the P. Therefore, P-C-type species might act as active sites where hydrogen atoms from water are attracted, chemisorbed (-P-C- + H-OH + e^- ⟶ -P-C(H)- + OH^-) and then reduced to hydrogen molecules (-P-C(H)- + H-OH + e^- ⟶ -P-C- + H_2 + OH^-). Despite the presence of P-C-type species in the carbon network, catalytic activity may be limited if these active sites are not exposed to the solution. This is observed in PA-700 and PA-800, which exhibit poor electrocatalytic performance due to the underdeveloped surface area, in spite of the large (P-$C_{species}$)/P_T. These results, along with our extensive characterization, suggest that the highest catalytic performance is obtained when P-C-type species are present, as well as a developed

porous texture. The conversion of P-O-type groups into P-C-type species is of paramount important for improving the catalytic activity of P-doped carbon materials for HER.

In addition, the stability of the most active electrocatalyst, PA-900, was also tested under working conditions after 1000 LSVs (Figure S6). As observed, this material shows excellent stability with cycling, which decreases only slightly after the electrochemical test. To further investigate the stability of the PA-900, chronoamperometric tests were performed under more aggressive conditions. As shown in Figure S7, PA-900 exhibits a catalytic retention of 60 % of the initial electrochemical activity after 5000 s, similar to that obtained by the commercial Pt/C (70 %) under similar conditions. The excellent performance of PA-900, along with its high stability under working and aggressive conditions, reinforce these PA-derived carbon materials as promising carbon-based HER electrocatalysts.

Furthermore, it is worth mentioning that the PA-900 catalyst competes with the most active metal-free electrocatalysts in the literature (Figure 6f and Table S2). It can be seen that PA-900 is indeed among the most efficient electrocatalysts based on heteroatom-doped and undoped carbon materials [69–73]. All materials that showed similar or better HER catalytic activity in Figure 6f and Table S2 were obtained from expensive carbon reagents, such as CNTs, hazardous products or complex and tedious synthesis routes, which leads to higher costs compared to the present PA-derived carbon materials. The synthesis of PA-900 is achieved in a one-step, low-cost and green synthesis through the heat treatment at 900 ºC of phytic acid, a biosourced material. This positions phytic acid-derived carbon materials as promising HER electrocatalysts to be improved and optimized with the aim of reaching platinum-like performance. Combining P-C-type species with other heteroatoms or defects may tune the chemical nature of the active sites and lead to an encouraging route to further enhance the catalytic activities of P-doped carbon materials for HER.

Conclusions

Phosphorus-doped carbon catalysts were successfully synthesized by a green and easy synthesis route based on phytic acid carbonization at different temperatures. The catalyst obtained by heat treatment at 900 ºC (PA-900) exhibits excellent HER performance (E_{HER} = -0.27 V), which is better than most heteroatom-doped, metal-free carbon materials in the literature. The extensive characterization of the P-doped carbons that have been prepared provides significant insight into the carbonization mechanisms for the conversion of phytic acid into P-doped carbon catalysts. The P-doped carbons obtained at the lowest temperatures show a predominance of polyphosphate groups (P-O) in the carbon structure, which are converted into P-C-type species at temperatures above 700 °C. The P-C-type content reaches a maximum at 900 ºC, which corresponds to the highest electrocatalytic activity of PA-900, suggesting that such P-C species are the most active functional groups in P-doped carbon materials for the HER. The electron-donating properties of phosphorus in the carbon structure is expected to produce a higher electron density in adjacent carbon atoms, resulting in higher reactivity of these carbon atoms and thus improving the catalytic performance towards HER. This work opens new perspectives to achieve better HER performance by combining P-C-type species with other heteroatoms or defects.

Author Contributions

SGD & JQB: conceptualization, investigation, methodology, writing – original draft; JCG, NB & MTI: investigation, writing – original draft; AC: validation, writing – review & editing, resources, supervision; VF: conceptualization, validation, writing – review & editing, resources, supervision, project administration, funding acquisition.

Acknowledgements

This study was partially supported by the French PIA project “Lorraine Université d’Excellence”, reference ANR-15-IDEX-04-LUE, and the TALiSMAN project funded by ERDF (2019-000214). SGD thanks the Ministerio de Universidades, the European Union, and the University of Oviedo for the financial support (MU-21-UP2021-030 30267158). JQB thanks the Ministerio de Universidades, the European Union, and the University of Alicante for the financial support (MARSALAS21-21).

References

[1] L. Chen, Z. Qi, S. Zhang, J. Su, G.A. Somorjai, Catalytic Hydrogen Production from Methane: A Review on Recent Progress and Prospect, Catalysts. 10 (2020). https://doi.org/https://doi.org/10.3390/catal10080858.

[2] X. Peng, S. Zhao, Y. Mi, L. Han, X. Liu, D. Qi, J. Sun, Y. Liu, H. Bao, L. Zhuo, H.L. Xin, J. Luo, Trifunctional Single-Atomic Ru Sites Enable Efficient Overall Water Splitting and Oxygen Reduction in Acidic Media, Small. 2002888 (2020) 1–10. https://doi.org/10.1002/smll.202002888.

[3] C. Zhang, H. Liu, Y. Liu, X. Liu, Y. Mi, R. Guo, J. Sun, H. Bao, J. He, Y. Qiu, J. Ren, X. Yang, J. Luo, G. Hu, Rh2S3/N-Doped Carbon Hybrids as pH-Universal Bifunctional Electrocatalysts for Energy-Saving Hydrogen Evolution, Small. 2000208 (2020) 1–11. https://doi.org/10.1002/smtd.202000208.

[4] H. Han, I. Kim, S. Park, Thermally template d cobalt oxide nanobubbles on crumple d graphene sheets : A promising non-precious metal catalysts for acidic oxygen evolution, Electrochim. Acta. 382 (2021) 138277. https://doi.org/10.1016/j.electacta.2021.138277.

[5] F. Cheng, J. Chen, Metal–air batteries: from oxygen reduction electrochemistry to cathode catalysts, Chem. Soc. Rev. (2012) 2172–2192. https://doi.org/10.1039/c1cs15228a.

[6] Z.-L. Wang, D. Xu, J.-J. Xu, X.-B. Zhang, Oxygen electrocatalysts in metal–air batteries: from aqueous to nonaqueous electrolytes, Chem. Soc. Rev. 43 (2013) 7746–7786. https://doi.org/10.1039/c3cs60248f.

[7] J. Stacy, Y.N. Regmi, B. Leonard, M. Fan, The recent progress and future of oxygen reduction reaction catalysis: A review, Renew. Sustain. Energy Rev. 69 (2017) 401–414. https://doi.org/10.1016/j.rser.2016.09.135.

[8] A. Morozan, B. Jousselme, S. Palacin, Low-platinum and platinum-free catalysts for the oxygen reduction reaction at fuel cell cathodes, Energy Environ. Sci. 4 (2011) 1238–1254. https://doi.org/10.1039/c0ee00601g.

[9] E.J. Popczun, C.G. Read, C.W. Roske, N.S. Lewis, R.E. Schaak, Highly Active Electrocatalysis of the Hydrogen Evolution Reaction by Cobalt Phosphide Nanoparticles, Angew. Chemie. (2014) 5531–5534. https://doi.org/10.1002/ange.201402646.

[10] B. Hinnemann, P.G. Moses, J. Bonde, K.P. Jørgensen, J.H. Nielsen, S. Horch, I. Chorkendorff, J.K. Nørskov, Biomimetic Hydrogen Evolution : MoS2 Nanoparticles as Catalyst for Hydrogen Evolution, J. Am. Chem. Soc. (2005) 5308–5309. https://doi.org/10.1021/ja0504690.

[11] C. Hu, H. Liu, Y. Liu, J.F. Chen, Y. Li, L. Dai, Graphdiyne with tunable activity towards hydrogen evolution reaction, Nano Energy. 63 (2019) 103874. https://doi.org/10.1016/j.nanoen.2019.103874.

[12] K. Zhang, Y. Zhang, Q. Zhang, Z. Liang, L. Gu, W. Guo, B. Zhu, S. Guo, R. Zou,

Metal- organic framework- derived Fe/Cu- substituted Co nanoparticles embedded in CNTs- grafted carbon polyhedron for Zn-air batteries, Carbon Energy. 2 (2020) 283–293. https://doi.org/10.1002/cey2.35.

[13] H. Li, Q. Li, P. Wen, T.B. Williams, S. Adhikari, C. Dun, C. Lu, D. Itanze, L. Jiang, D.L. Carroll, G.L. Donati, P.M. Lundin, Y. Qiu, S.M. Geyer, Colloidal Cobalt Phosphide Nanocrystals as Trifunctional Electrocatalysts for Overall Water Splitting Powered by a Zinc–Air Battery, Adv. Mater. 30 (2018) 1705796. https://doi.org/10.1002/adma.201705796.

[14] S. Li, C. Cheng, X. Zhao, J. Schmidt, A. Thomas, Active Salt/Silica- Templated 2D Mesoporous FeCo- Nx- Carbon as Bifunctional Oxygen Electrodes for Zinc-Air Batteries, Angew. Chemie - Int. Ed. 57 (2018) 1856–1862. https://doi.org/10.1002/anie.201710852.

[15] J. Quílez-Bermejo, S. García-Dalí, A. Daouli, A. Zitolo, R.L.S. Canevesi, M. Emo, M.T. Izquierdo, M. Badawi, A. Celzard, V. Fierro, Advanced Design of Metal Nanoclusters and Single Atoms Embedded in C1N1-Derived Carbon Materials for ORR, HER, and OER, Adv. Funct. Mater. 2300405 (2023). https://doi.org/10.1002/adfm.202300405.

[16] J. Masa, W. Xia, M. Muhler, W. Schuhmann, On the Role of Metals in Nitrogen- Doped Carbon Electrocatalysts for Oxygen Reduction, Angew. Chemie - Int. Ed. 54 (2015) 10102–10120. https://doi.org/10.1002/anie.201500569.

[17] H.T. Chung, D.A. Cullen, D. Higgins, B.T. Sneed, E.F. Holby, K.L. More, P. Zelenay, Direct atomic-level insight into the active sites of a high-performance PGM-free ORR catalyst, Science. 357 (2017) 479–484. https://doi.org/10.1126/science.aan2255.

[18] Z. Zhao, Z. Yuan, Z. Fang, J. Jian, J. Li, M. Yang, C. Mo, Y. Zhang, X. Hu, P. Li, S. Wang, W. Hong, Z. Zheng, G. Ouyang, X. Chen, D. Yu, In Situ Activating Strategy to Significantly Boost Oxygen Electrocatalysis of Commercial Carbon Cloth for Flexible and Rechargeable Zn-Air Batteries, Adv. Sci. 5 (2018) 1800760. https://doi.org/10.1002/advs.201800760.

[19] R. Paul, Q. Dai, C. Hu, L. Dai, Ten years of carbon- based metal- free electrocatalysts, Carbon Energy. 1 (2019) 19–31. https://doi.org/10.1002/cey2.5.

[20] J. Quílez-Bermejo, M. Melle-Franco, E. San-Fabián, E. Morallón, D. Cazorla-Amorós, Towards understanding the active sites for the ORR in N-doped carbon materials through fine-tuning of nitrogen functionalities: An experimental and computational approach, J. Mater. Chem. A. 7 (2019) 24239–24250. https://doi.org/10.1039/c9ta07932g.

[21] Z. Duan, G. Henkelman, Identification of Active Sites of Pure and Nitrogen-Doped Carbon Materials for Oxygen Reduction Reaction Using Constant-Potential Calculations, J. Phys. Chem. C. 124 (2020) 12016–12023. https://doi.org/10.1021/acs.jpcc.0c03951.

[22] A.R. Ferens, R.D. Weinstein, R. Giuliano, J.A. Hull, Selective decomposition of isopropanol using as prepared and oxidized graphite nanofibers, Carbon. 50 (2011) 192–200. https://doi.org/10.1016/j.carbon.2011.08.020.

[23] F. Rodriguez-Reinoso, M. Molina-Sabio, M.A. Munecas, Effect of Microporosity and Oxygen

Surface Groups of Activated Carbon in the Adsorption of Molecules of Different Polarity, J. Phys. Chem. (1992) 2707–2713.

[24] W. Kiciński, M. Szala, M. Bystrzejewski, Sulfur-doped porous carbons: Synthesis and applications, Carbon. 68 (2014) 1–32. https://doi.org/10.1016/j.carbon.2013.11.004.

[25] T.J. Bandosz, T.Z. Ren, Porous carbon modified with sulfur in energy related applications, Carbon. 118 (2017) 561–577. https://doi.org/10.1016/j.carbon.2017.03.095.

[26] T. Nakajima, Surface Modification of Carbon Anodes for Lithium Ion Batteries by Fluorine and Chlorine, Elsevier, 2015. https://doi.org/10.1016/B978-0-12-800679-5.00009-9.

[27] P. Barpanda, G. Fanchini, G.G. Amatucci, Structure, surface morphology and electrochemical properties of brominated activated carbons, Carbon. 49 (2011) 2538–2548. https://doi.org/10.1016/j.carbon.2011.02.028.

[28] J. Quílez-Bermejo, E. Morallón, D. Cazorla-Amorós, Metal-free heteroatom-doped carbon-based catalysts for ORR. A critical assessment about the role of heteroatoms, Carbon. 165 (2020) 434–454. https://doi.org/10.1016/j.carbon.2020.04.068.

[29] Y. Wen, B. Wang, C. Huang, L. Wang, D. Hulicova-Jurcakova, Synthesis of Phosphorus- Doped Graphene and its Wide Potential Window in Aqueous Supercapacitors, Chem. - A Eur. J. 21 (2015) 80–85. https://doi.org/10.1002/chem.201404779.

[30] R. Berenguer, R. Ruiz-Rosas, A. Gallardo, D. Cazorla-Amorós, E. Morallón, H. Nishihara, T. Kyotani, J. Rodríguez-Mirasol, T. Cordero, Enhanced electro-oxidation resistance of carbon electrodes induced by phosphorus surface groups, Carbon. 95 (2015) 681–689. https://doi.org/10.1016/j.carbon.2015.08.101.

[31] E.H. Ramírez-Soria, S. García-Dalí, J.M. Munuera, D.F. Carrasco, S. Villar-rodil, J.M.D. Tascón, J.I. Paredes, J. Bonilla-cruz, A Simple and Expeditious Route to Phosphate-Functionalized, Water-Processable Graphene for Capacitive Energy Storage, ACS Appl. Mater. Interfaces. 13 (2021) 54860–54873. https://doi.org/10.1021/acsami.1c12135.

[32] B. Martínez-Sánchez, D. Cazorla-Amorós, E. Morallón, P-functionalized carbon nanotubes promote highly stable electrocatalysts based on Fe-phthalocyanines for oxygen reduction: Experimental and computational studies, J. Energy Chem. 72 (2022) 276–290. https://doi.org/10.1016/j.jechem.2022.05.024.

[33] J. Zhang, Z. Zhao, Z. Xia, L. Dai, A metal-free bifunctional electrocatalyst for oxygen reduction and oxygen evolution reactions, Nat. Nanotechnol. 10 (2015) 444–452. https://doi.org/10.1038/nnano.2015.48.

[34] M. Enterría, J.L. Figueiredo, Nanostructured mesoporous carbons : Tuning texture and surface chemistry, Carbon N. Y. 108 (2016) 79–102. https://doi.org/10.1016/j.carbon.2016.06.108.

[35] H. Benaddi, D. Legras, J.N. Rouzaud, F. Beguin, Influence of the atmosphere in the chemical activation of wood by phosphoric acid, Carbon. (1998) 306–309. https://doi.org/10.1016/S0008-6223(98)80123-1.

[36] P. Wang, H. He, X. Xu, Y. Jin, Significantly Enhancing Supercapacitive Performance of Nitrogen- doped Graphene Nanosheet Electrodes by Phosphoric Acid Activation, ACS Appl. Mater. Interfaces. 6 (2014) 1563–1568. https://doi.org/10.1021/am404277j.

[37] M. Rusop, T. Soga, T. Jimbo, Photovoltaic characteristics of phosphorus-doped amorphous carbon films grown by r.f. plasma-enhanced CVD, Sol. Energy Mater. Sol. Cells. 90 (2006) 3214–3222. https://doi.org/10.1016/j.solmat.2006.06.017.

[38] J. Quílez-Bermejo, S. Pérez-Rodríguez, A. Celzard, V. Fierro, Progress in the Use of Biosourced Phenolic Molecules for Electrode Manufacturing, Front. Mater. 9 (2022) 1–18. https://doi.org/10.3389/fmats.2022.810575.

[39] M.A. Patel, F. Luo, M.R. Khoshi, E. Rabie, Q. Zhang, C.R. Flach, R. Mendelsohn, E. Garfunkel, M. Szostak, H. He, P‐Doped Porous Carbon as Metal Free Catalysts for Selective Aerobic Oxidation with an Unexpected Mechanism, ACS Nano. 10 (2016) 2305–2315. https://doi.org/10.1021/acsnano.5b07054.

[40] M. Thommes, K. Kaneko, A. V. Neimark, J.P. Olivier, F. Rodriguez-Reinoso, J. Rouquerol, K.S.W. Sing, Physisorption of gases, with special reference to the evaluation of surface area and pore size distribution (IUPAC Technical Report), Pure Appl. Chem. 87 (2015) 1051–1069. https://doi.org/10.1515/pac-2014-1117.

[41] P. Mallet-Ladeira, P. Puech, C. Toulouse, M. Cazayous, N. Ratel-Ramond, P. Weisbecker, G.L. Vignoles, M. Monthioux, A Raman study to obtain crystallite size of carbon materials: A better alternative to the Tuinstra-Koenig law, Carbon. 80 (2014) 629–639. https://doi.org/10.1016/j.carbon.2014.09.006.

[42] L. Bouleau, S. Pérez-Rodríguez, J. Quílez-Bermejo, M.T. Izquierdo, F. Xu, V. Fierro, A. Celzard, Best practices for ORR performance evaluation of metal-free porous carbon electrocatalysts, Carbon. 189 (2022) 349–361. https://doi.org/10.1016/j.carbon.2021.12.078.

[43] J. Castro-Gutiérrez, N. Díez, M. Sevilla, M.T. Izquierdo, J. Ghanbaja, A. Celzard, V. Fierro, High-Rate Capability of Supercapacitors Based on Tannin-Derived Ordered Mesoporous Carbons, ACS Sustain. Chem. Eng. 7 (2019) 17627–17635. https://doi.org/10.1021/acssuschemeng.9b03407.

[44] M. Okamura, A. Takagaki, M. Toda, J.N. Kondo, K. Domen, T. Tatsumi, M. Hara, S. Hayashi, Acid-catalyzed reactions on flexible polycyclic aromatic carbon in amorphous carbon, Chem. Mater. 18 (2006) 3039–3045. https://doi.org/10.1021/cm0605623.

[45] S. Bernard, O. Beyssac, K. Benzerara, N. Findling, G. Tzvetkov, G.E. Brown, XANES, Raman and XRD study of anthracene-based cokes and saccharose-based chars submitted to high-temperature pyrolysis, Carbon. 48 (2010) 2506–2516. https://doi.org/10.1016/j.carbon.2010.03.024.

[46] A.C. Ferrari, J. Robertson, Interpretation of Raman spectra of disordered and amorphous carbon, Phys. Rev. B. 61 (1999) 14095–107. https://doi.org/10.1007/BF02543692.

[47] A.C. Ferrari, J. Robertson, Raman spectroscopy of amorphous, nanostructured, diamond-like carbon, and nanodiamond, Philos. Trans. R. Soc. A. 2 (2004) 2477–2512. https://doi.org/10.1098/rsta.2004.1452.

[48] X. Wu, L.R. Radovic, Inhibition of catalytic oxidation of carbon/carbon composites by phosphorus, Carbon. 44 (2006) 141–151. https://doi.org/10.1016/j.carbon.2005.06.038.

[49] S.K. Jerng, D.S. Yu, J.H. Lee, C. Kim, S. Yoon, S.H. Chun, Graphitic carbon growth on crystalline and amorphous oxide substrates using molecular beam epitaxy, Nanoscale Res. Lett. 6 (2011) 1–6. https://doi.org/10.1186/1556-276X-6-565.

[50] J. Xu, L. Chen, H. Qu, Y. Jiao, J. Xie, Preparation and characterization of activated carbon from reedy grass leaves by chemical activation with H3PO4, Appl. Surf. Sci. 320 (2014) 674–680. https://doi.org/10.1016/j.apsusc.2014.08.178.

[51] J. Wu, X. Zheng, C. Jin, J. Tian, R. Yang, Ternary doping of phosphorus, nitrogen, and sulfur into porous carbon for enhancing electrocatalytic oxygen reduction, Carbon. 92 (2015) 327–338. https://doi.org/10.1016/j.carbon.2015.05.013.

[52] V. Sydorchuk, O.I. Poddubnaya, M.M. Tsyba, O. Zakutevskyy, O. Khyzhun, S. V Khalameida, A.M. Puziy, Photocatalytic degradation of dyes using phosphorous-containing activated carbons, Appl. Surf. Sci. 535 (2021) 147667. https://doi.org/10.1016/j.apsusc.2020.147667.

[53] N. Baccile, C. Falco, M.M. Titirici, Characterization of biomass and its derived char using 13C-solid state nuclear magnetic resonance, Green Chem. 16 (2014) 4839–4869. https://doi.org/10.1039/c3gc42570c.

[54] B. Cade-Menun, C.W. Liu, Solution Phosphorus-31 Nuclear Magnetic Resonance Spectroscopy of Soils from 2005 to 2013: A Review of Sample Preparation and Experimental Parameters, Soil Sci. Soc. Am. J. 78 (2014) 19–37. https://doi.org/10.2136/sssaj2013.05.0187dgs.

[55] P. Sannigrahi, E. Ingall, Polyphosphates as a source of enhanced P fluxes in marine sediments overlain by anoxic waters: Evidence from 31P NMR, Geochem. Trans. 6 (2005) 52–59. https://doi.org/10.1063/1.1946447.

[56] A.J.R. Costello, T. Glonek, T.C. Myers, 31P Nuclear magnetic resonance-pH titrations of myo-inositol hexaphosphate, Carbohydr. Res. 46 (1976) 159–171. https://doi.org/10.1016/S0008-6215(00)84287-1.

[57] R. Fu, L. Liu, W. Huang, P. Sun, Studies on the Structure of Activated Carbon Fibers Activated by Phosphoric Acid, J. Appl. Polym. Sci. 87 (2003) 2253–2261. https://doi.org/10.1002/app.11607.

[58] G.A. Naikoo, M. Thomas, M. Anis Ganaie, M.U.D. Sheikh, M. Bano, I.U. Hassan, F. Khan, Hierarchically macroporous silver monoliths using Pluronic F127: Facile synthesis, characterization and its application as an efficient biomaterial for pathogens, J. Saudi Chem. Soc. 20 (2016) 237–244. https://doi.org/10.1016/j.jscs.2015.12.002.

[59] M. Jagtoyen, F. Derbyshire, Activated carbons from yellow poplar and white oak by H3PO4 activation, Carbon. 36 (1998) 1085–1097. https://doi.org/10.1016/S0008-6223(98)00082-7.

[60] A.L.M. Daneluti, J. do R. Matos, Study of thermal behavior of phytic acid, Brazilian J. Pharm. Sci. 49 (2013) 275–283. https://doi.org/10.1590/S1984-82502013000200009.

[61] Z. Jiang, G. Liu, Microencapsulation of ammonium polyphosphate with melamine-formaldehyde-tris(2-hydroxyethyl)isocyanurate resin and its flame retardancy in polypropylene, RSC Adv. 5 (2015) 88445–88455. https://doi.org/10.1039/c5ra14586d.

[62] J.L. Figueiredo, M.F.R. Pereira, M.M.A. Freitas, J.J.M. Órfão, Modification of the surface chemistry of activated carbons, Carbon. 37 (1999) 1379–1389. https://doi.org/10.1016/S0008-6223(98)00333-9.

[63] F.J. García-Mateos, J.M. Rosas, R. Ruiz-Rosas, J. Rodríguez-Mirasol, T. Cordero, Highly porous and conductive functional carbon fibers from electrospun phosphorus-containing lignin fibers, Carbon. 200 (2022) 134–148. https://doi.org/10.1016/j.carbon.2022.08.050.

[64] M.J. Valero-Romero, F.J. García-Mateos, J. Rodríguez-Mirasol, T. Cordero, Role of surface phosphorus complexes on the oxidation of porous carbons, Fuel Process. Technol. 157 (2017) 116–126. https://doi.org/10.1016/j.fuproc.2016.11.014.

[65] K.S. Lee, Y.J. Seo, H.T. Jeong, Capacitive behavior of functionalized activated carbon-based all-solid-state supercapacitor, Carbon Lett. 31 (2021) 1041–1049. https://doi.org/10.1007/s42823-020-00219-w.

[66] B.E. Conway, Electrochemical Supercapacitors: Scientific Fundamentals and Technological Applications, Kluwer Academic/Plenum Publishers, New York, 1999. https://doi.org/10.1007/978-1-4757-3058-6.

[67] J. Quílez-Bermejo, K. Strutyński, M. Melle-Franco, E. Morallón, D. Cazorla-Amorós, On the Origin of the Effect of pH in Oxygen Reduction Reaction for Nondoped and Edge-Type Quaternary N-Doped Metal-Free Carbon-Based Catalysts, ACS Appl. Mater. Interfaces. 12 (2020) 54815–54823. https://doi.org/10.1021/acsami.0c17249.

[68] J.X. Flores-Lasluisa, J. Quílez-Bermejo, A.C. Ramírez-Pérez, F. Huerta, D. Cazorla-amor, E. Morall, Copper-Doped Cobalt Spinel Electrocatalysts on Activated Carbon for Hydrogen Evolution Reaction, Materials (Basel). 12 (2019) 1302. https://doi.org/10.3390/ma12081302.

[69] J. Zhao, Z. Pu, H. Jin, Z. Zhang, J. Liu, S. Mu, Phosphorous-doped carbon coordinated iridium diphosphide bifunctional catalyst with ultralow iridium amount for efficient all-pH-value hydrogen evolution and oxygen reduction reactions, J. Catal. 383 (2020) 244–253. https://doi.org/10.1016/j.jcat.2020.01.026.

[70] Z. Liu, J. Ai, M. Sun, F. Han, Z. Li, Q. Peng, Q. De Wang, J. Liu, L. Liu, Phosphorous-Doped Graphite Layers with Outstanding Electrocatalytic Activities for the Oxygen and Hydrogen Evolution Reactions in Water Electrolysis, Adv. Funct. Mater. 30 (2020). https://doi.org/10.1002/adfm.201910741.

[71] Y. Lei, M. Jia, P. Guo, J. Liu, J. Zhai, MoP nanoparticles encapsulated in P-doped carbon as an efficient electrocatalyst for the hydrogen evolution reaction, Catal. Commun. 140 (2020) 106000. https://doi.org/10.1016/j.catcom.2020.106000.

[72] Y. Wen, S. Xu, P. Wang, X. Shao, X. Sun, J. Hu, X.R. Shi, Bimetallic FeCo phosphide nanoparticles anchored on N-doped carbon foam for wide pH hydrogen evolution reaction, J. Alloys Compd. 931 (2023) 167570. https://doi.org/10.1016/j.jallcom.2022.167570.

[73] Y. Zhang, Y. Tan, X. Wang, L. Dong, A. Liu, Hybrid of NiO-Ni12P5/N-doped carbon nanotubes as non-noble electrocatalyst for efficient hydrogen evolution reaction, Colloids Surfaces A Physicochem. Eng. Asp. 608 (2021) 125613. https://doi.org/10.1016/j.colsurfa.2020.125613.